Noncovalent Interactions in the Gas Phase: The Anisole–Phenol Complex

9 **AUTHORS**, INCLUDING:

Giangaetano Pietraperzia
University of Florence
52 PUBLICATIONS **541** CITATIONS

SEE PROFILE

Malgorzata Biczysko
Shanghai University
84 PUBLICATIONS **1,725** CITATIONS

SEE PROFILE

Julien Bloino
Italian National Research Council
67 PUBLICATIONS **1,911** CITATIONS

SEE PROFILE

Vincenzo Barone
Scuola Normale Superiore di Pisa
774 PUBLICATIONS **44,791** CITATIONS

SEE PROFILE

Noncovalent Interactions in the Gas Phase: The Anisole−Phenol Complex

Giangaetano Pietraperzia,*[,†,‡] Massimiliano Pasquini,[†,‡] Federico Mazzoni,[†,‡] Giovanni Piani,[†,⊥] Maurizio Becucci,[†,‡] Malgorzata Biczysko,*[,§,‖] Daniel Michalski,[‖] Julien Bloino,[§,‖] and Vincenzo Barone[§]

[†]LENS, Polo Scientifico e Tecnologico dell'Università di Firenze, Via Nello Carrara 1, 50019 Sesto Fiorentino (FI), Italy

[‡]Dipartimento di Chimica, Polo Scientifico e Tecnologico dell'Università di Firenze, Via della Lastruccia 3, 50019 Sesto Fiorentino (FI), Italy

[§]Scuola Normale Superiore di Pisa and INFN Sezione di Pisa, Piazza dei Cavalieri 7, 56126 Pisa, Italy

[‖]Department of Chemistry "P. Corradini", Università di Napoli "Federico II" and INSTM "M³-Village", Complesso Universitario Monte Sant'Angelo, Via Cintia, 80126 Naples, Italy

Ⓢ *Supporting Information*

ABSTRACT: The present paper reports on an integrated spectroscopic study of the anisole−phenol complex in a molecular beam environment. Combining REMPI and HR-LIF spectroscopy experimental data with density functional computations (TD-M05-2X/M05-2X//N07D) and first principle spectra simulations, it was possible to locate the band origin of the $S_1 \leftarrow S_0$ electronic transition and determine the equilibrium structure of the complex, both in the S_0 and S_1 electronic states. Experimental and computational evidence indicates that the observed band origin is due to an electronic transition localized on the phenol frame, while it was not possible to localize experimentally another band origin due to the electronic transition localized on the anisole molecule. The observed structure of the complex is stabilized by a hydrogen bond between the phenol, acting as a proton donor, and the anisole molecule, acting as an acceptor through the lone pairs of the oxygen atom. A secondary interaction involving the hydrogen atoms of the anisole methyl group and the π electron system of the phenol molecule stabilizes the complex in a nonplanar configuration. Additional insights about the landscapes of the potential energy surfaces governing the ground and first excited electronic states of the anisole−phenol complex, with the issuing implications on the system photodynamic, can be extracted from the combined experimental and computational studies.
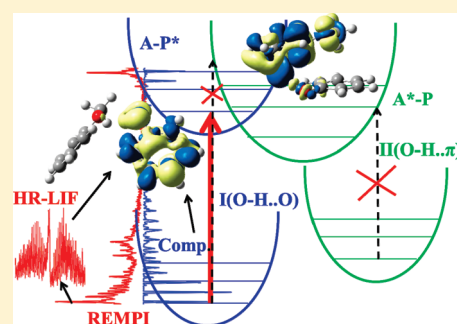
■ INTRODUCTION

Noncovalent interactions play a remarkable role in many areas of chemistry, biology, and materials science,[1−3] and in particular, $\pi-\pi$ stacking is fundamental to understand and explain many supramolecular organization and recognition processes.[4] It is important for base pairing in the DNA supramolecular structure, side-chain interactions in proteins, host−guest chemistry, self-assembly based on synthetic molecules, and intercalation of certain drugs into the DNA. In the last years those topics received a lot of attention because a deeper understanding of elementary interactions governing nanorecognition is of fundamental importance for the design of novel supramolecular systems and nanomaterials and for the elucidation of the fundamental mechanisms by which proteins perform their function.[5−13]

Probably the first investigations on stacking interactions were performed for the benzene dimer, which, due to the lack of any concurrent specific interaction, seemed to be the best candidate for this kind of study. Actually, several possible relative orientations of benzene units are possible, leading to the presence of stacked, displaced stacked, and T-shaped structures. Quantum mechanical computations of increasing accuracy indicate that the

latter two structures are the most stable, but only the T-shaped configuration has been observed experimentally.[14] Its stability is due to quadrupole−quadrupole interactions, which are repulsive for parallel aromatic rings, but become an attractive force for the T-shaped structure.[15]

Substituents may alter the energy landscape through both electron localization and delocalization contributions issuing from inductive effects related to the substituent electronegativity and to resonance effects. In the case of the toluene dimer in both aqueous solutions and gas phase, the two stacked configurations are predicted to be more stable than the T-shaped one.[16,17] Toluene dimer has been experimentally studied by means of REMPI, hole-burning, and stimulated Raman−UV double resonance spectroscopies.[18] The REMPI spectrum presented very broad and not structured bands. Using double resonance

methods, two band systems have been suggested, although the underlying evidence is not completely clear. The authors invoke three possible different explanations for this experimental outcome. The first one is related to the potential presence of transitions due to different isomers of the dimer. The second one relies on the overlapping of low frequency vibronic transitions, with a simultaneous dramatic structural change and a very short lifetime in the excited S_1 state. The last possibility suggests that hot bands have been observed. Theoretical studies[16,17] have evidenced some differences between the toluene and benzene dimers. The toluene dimer prefers a stacked conformation because the dipole—dipole attractive interaction overwhelms the repulsive quadrupole—quadrupole one.

Concerning other aromatic systems, an OH group monosubstitution in the benzene dimer (benzene—phenol complex) leads also to a change from a T-shaped to a stacked structure, while in the case of the phenol dimer and trimer, the main stabilizing interaction becomes an intermolecular hydrogen bond. As a matter of fact, for the latter dimer a strong interaction between the two OH groups takes place, leading to a completely different structure, in which the two phenol molecules are more or less coplanar, with one of them acting as an acid (proton donor), and the second one acting as a base (proton acceptor). The formation of a hydrogen bond involving both phenol molecules has been highlighted by spectroscopic measurements,[19] and REMPI spectra show two different origins for electronic transitions corresponding to the $S_1 \leftarrow S_0$ band system of the monomer. A first set of bands is related to the transition localized on the proton donor phenol: this can be recognized from the red shift with respect to the bare phenol, analogous to the one observed in the phenol—water complex.[20] The second series, instead, is blue-shifted and is assigned to the electronic transition localized on the proton acceptor phenol. However, while H-bonding rules the structure of the complex, the $\pi-\pi$ interaction still plays a significant role. If only hydrogen bond was present the two phenol aromatic rings should lie in the same plane, placed in a trans configuration with respect to the $O-H\cdots O$ bond axis. Instead, the measured rotational constants[21] suggest a more compact structure, with the two aromatic rings involved in an attractive interaction. The $\pi-\pi$ interaction becomes even more significant with the phenol trimer.[22]

Recently Schmitt et al. determined the intermolecular structure of the phenol dimer in the S_0 and S_1 electronic states by means of rotationally resolved electronic spectroscopy.[23] Their results substantially agree with previously published studies: the intermolecular structure in the electronic ground state is described as hydrogen bonded, one phenol molecule acting as a proton donor with respect to the other. The structure presents a deviation from a pure linear arrangement, due to dispersion interactions, but the experimental rotational constants of five isotopomers combined with semiempirical modeling were not sufficient for an unambiguous determination of the whole structure of the dimer in the S_1 electronic state. However, further dispersed fluorescence (DF) spectra combined with refined quantum mechanical (QM) computations and fitting of seven vibronic bands led to a fully consistent picture characterized by significant geometry changes in the donor moiety and an essentially unmodified acceptor moiety with respect to the structure of the ground electronic state.[24]

Our groups have performed several studies related to noncovalent interactions in the gas phase, in particular for molecular complexes involving anisole,[25-27] including the anisole dimer.[28,29] The latter complex is strongly related to the phenol dimer, but without the possibility of classical hydrogen bond formation, so that the equilibrium structure of the complex needs to be governed by a subtle balance between different contributions. For such reasons the structure of anisole dimer could not be easily predicted a priori, and this complex has been considered also as a challenging test for quantum mechanical (QM) computations.[28] With a series of combined experimental and theoretical studies it was possible to put in evidence that the anisole dimer is stabilized mainly by dispersive interactions, resulting in a center-symmetric displaced stacked equilibrium configuration.[28,29] The anisole dimer is the first example of a stacked dimer observed experimentally under high-resolution conditions. Moreover, while studying some deuterated anisole species and mixed complexes, it was possible to highlight some influence of excitonic interactions on the first excited singlet electronic state of the anisole dimer.[29]

In the present work we are continuing integrated experimental and computational studies on the noncovalent interactions by presenting the results on the mixed cluster between anisole and phenol molecules. The anisole molecule is able to act as a proton acceptor only, so we expect that the equilibrium structure of the mixed dimer should involve a hydrogen bond between the proton donor phenol and the proton acceptor anisole. Both experimental (REMPI, HR-LIF experiments) and theoretical (DFT/TD-DFT calculations, spectra simulation) techniques have been used to gain further insights on the structure, nature of intermolecular interactions, and spectroscopic properties of the anisole—phenol dimer.

■ EXPERIMENTAL SECTION

REMPI and HR-LIF experiments have been performed using the spectrometers installed at LENS and already described in detail in previous works.[30,31]

For the REMPI experiment, a gas mixture containing anisole and phenol (with helium as carrier gas) is allowed to expand in a vacuum chamber maintained at 10^{-4} mbar during normal operation, then with a conical skimmer, we select the central part of the expansion and let it enter a differentially pumped vacuum chamber, which constitutes the interaction region, where the pressure is maintained at a lower value (10^{-6} mbar). The source is a pulsed valve with a 10 Hz repetition rate and with a nozzle diameter of 500 μm. Typical opening times of the pulsed valve are 200 μs. Helium is flowing into two different reservoirs in which anisole and phenol are maintained unmixed. It is possible to keep the two samples at different temperatures in order to control the composition of the expanding mixture: typically, anisole is maintained at a temperature of 263 K and phenol at 308 K; the nozzle is heated at 313 K. The backing pressure used to maximize the anisole-phenol formation under these conditions is 3 bar. The laser source is a Nd:YAG pumped dye laser, operating with Coumarin 153 dye. The laser bandwidth is narrower than 0.1 cm^{-1}. The fundamental emission generated by the dye laser is then frequency doubled in a BBO crystal. The signal is collected using a real time MCP gain control strategy.[32]

The HR-LIF experiment is performed using a continuous wave (CW) molecular beam source with a 100 μm diameter nozzle and a conical skimmer (Beam Dynamics model 2, 400 μm diameter) placed at 10 mm downstream from the nozzle. The expanding mixture is the same as the one used in the REMPI experiment, except for the different temperatures of the two

9604

dx.doi.org/10.1021/jp200444a |*J. Phys. Chem. A* 2011, 115, 9603–9611

samples (phenol was maintained at 313 K and anisole at 293 K). The pressure in the interaction chamber is below 10^{-6} mbar. The laser radiation is generated with a CW, single mode, frequency stabilized, ring dye laser (Coherent 699−21) operating with Rhodamine110 dye, pumped at 515 nm with 6 W power, and frequency doubled in an external optical resonator (LAS Wavetrain) with a BBO crystal: we are able to generate up to 16 mW of laser power at 276 nm. Around the excitation wavelength, the spectral instrumental function of our apparatus is Gaussian, about 30 MHz fwhm, mainly attributed to residual Doppler broadening associated to the divergence of the molecular beam.

■ COMPUTATIONAL STRATEGIES

A reliable study of the anisole−phenol complex in the ground and excited electronic states requires a proper account of all possible weak intermolecular interactions, including the stacking one. Recently we have shown that, among a large number of tested DFT/TD-DFT models, the M05-2X functional[33] and its time-dependent counterpart provide the best agreement between experimental and computed geometric structures in both the ground and first excited electronic states for π-stacked anisole dimer.[28,29] Moreover, extended benchmark studies showed that M05-2X describes accurately both noncovalent interactions and excitations energies.[34−36] In the present work a more recent functional from the Minnesota family, M06-2X,[37] has been also considered, leading however to a worse agreement between computed and experimental rotational constants (mean absolute deviation in the ground and excited states of 5% and 7.5% over 2.5% and 3.2% for M06-2X and M05-2X, respectively, vide infra). For such reasons the M05-2X functional has been chosen also in the current work. This functional has been combined with the recently introduced N07D double-ζ basis set[38−40] built by adding a reduced number of polarization and diffuse functions to the 6-31G set and coupling a remarkable reliability in the computation of spectroscopic properties with a very favorable scaling with the number of electrons in term of computational costs. In the current study the original N07D basis set has been augmented by a single set of s diffuse functions on the carbon atoms (C-Diff) as recommended in the recent work on the excited state properties of vinyl radical.[41] Thus all geometry optimizations and frequency computations have been performed at M05-2X/N07D(C-Diff) and TD-M05-2X/N07D(C-Diff) levels for the ground and excited electronic states, respectively. The TD-DFT harmonic frequencies have been evaluated by numerical differentiation of analytical energy gradients.[42] Additionally, the effect of the basis set extension on both ground and excited state energetic properties has been evaluated through single point M05-2X and TD-M05-2X computations in conjunction with a basis set of triple-ζ quality (aug-N07T[40]). For both ground and excited electronic states the BSSE (basis set superposition error) has been taken into account via the counterpoise correction (CP) to the interaction energies. In the latter case BSSE corrections have been computed assuming the excitation to be localized on one of the aromatic frames, in particular the counterpoise (CP) corrected binding energies have been calculated according to the scheme

$$\Delta E_{CP}^{*}(AB) = [E_{AB}^{AB}(AB)^{*} - E_{A}^{A}(A)^{*} - E_{B}^{B}(B)] +$$

$$[E_{AB}^{A}(A)^{*} + E_{AB}^{B}(B) - E_{AB}^{A}(A)^{*} - E_{AB}^{AB}(B)]$$

where $E_{X}^{Y}(Z)$ is the energy of subsystem Z at geometry X with basis set Y, A and B correspond to excited (A) and spectator (B) aromatic frames respectively, excited state calculations are labeled by the asterisk (*).

Vibrationally resolved electronic spectra have been simulated through an integrated procedure (described in detail elsewhere[43,44]) based on the computation of overlap integrals, also known as Franck−Condon (FC) integrals, between the vibrational wave functions of the electronic states involved in the transition. Both adiabatic and vertical approaches have been applied to simulate the one-photon absorption (OPA) spectrum. Within the adiabatic−Hessian (AH) framework, the evaluation of the FC integrals requires the computation of the equilibrium geometry structures and the vibrational properties of both electronic states and takes into account changes in the vibrational frequencies and mixing between the normal modes of the initial and final states (Duschinsky rotation[45]), $\mathbf{Q}^{i} = \mathbf{J}\mathbf{Q}^{f} + \mathbf{K}$, where $\mathbf{Q}^{i}$ and $\mathbf{Q}^{f}$ represent the mass-weighted normal coordinates of the initial and final electronic states, respectively. The Duschinsky matrix $\mathbf{J}$ describes the rotation of the normal coordinate basis vectors of the initial state during the transition. The shift vector $\mathbf{K}$ represents the displacement of the normal modes between the initial- and final-state structures. The applied approach is based on an a priori selection scheme to choose and then compute all the non-negligible transitions,[46,47] which has proven to provide very accurate spectra of medium-to-large systems with a limited computational cost.[43,44] Moreover, a simplified procedure set within the vertical model, where the harmonic PES of the final state is evaluated at the equilibrium geometry of the initial state, has been applied.[44] It assumes that the Hessian matrix is the same in both initial and final states, so that the changes in the normal modes during the transitions are only accounted by the shift vector $\mathbf{K}$ extrapolated from the energy gradient of the final state at the equilibrium geometry of the initial one. Such a model, which we will refer to as vertical gradient (VG), is also known in literature as the linear coupling model[48] (LCM) and allows a simplified simulation of the overall spectra shape. Computations of FC integrals within VG and AH frameworks (denoted as FC|VG and FC|AH, respectively) provide information on the probability and intensity of transitions, and this aspect will be extensively exploited in the current work.

The nature of the electronic transitions has been investigated by natural bond orbital (NBO) analyses[49] of the electronic densities for the ground and excited states. All calculations were performed with a locally modified version of the GAUSSIAN suite of quantum chemistry programs.[50]

■ EXPERIMENTAL RESULTS

We have measured the REMPI spectrum of the anisole−phenol complex in quite a broad spectral region trying to identify the presence of different conformers and the presence of two different electronic excited states, corresponding to excitation localized in either the phenol or anisole unit. The origin of the $S_1 \leftarrow S_0$ electronic transition has been located at 35996.99 cm^{-1}, showing a red shift with respect to the band origins of both monomers (36384.19 cm^{-1} for anisole and 36348.72 cm^{-1} for phenol). Despite an extended search, from 34800 to 37380 cm^{-1} (corresponding to 287.3−267.5 nm) we have found evidence for a single origin band. Figure 1 shows the REMPI spectrum for the anisole−phenol cluster parent ion in the region 34800−36500 cm^{-1} (287.3−274.2 nm); the assigned
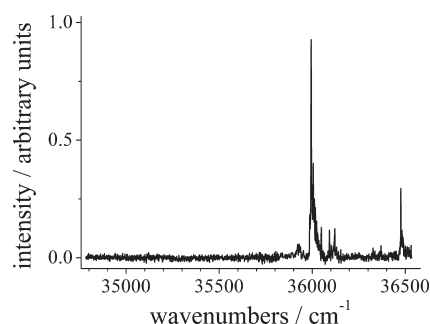
Figure 1. REMPI spectrum of the anisole—phenol complex around the band origin, located at about 36000 cm^{-1}. The absence of any further band origin in the red wing (starting from 34800 cm^{-1}) is apparent (see main text for details). The spectrum shows several vibronic bands due to the intermolecular motion of the two monomers blue shifted with respect to the transition origin.
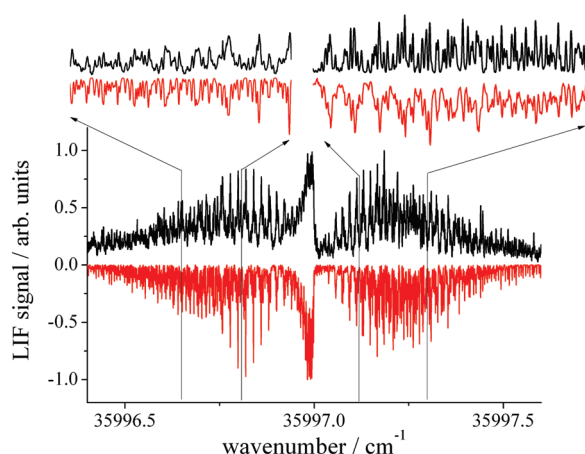

Figure 2. HR-LIF spectrum of the band origin of the anisole—phenol complex. The lower inverted trace is the spectrum simulated with parameters obtained from the fitting procedure of the experimental spectrum. The two insets show details of the P and R branches of the band.

Table 1. Experimental Rotational Constants for the Anisole—Phenol Dimer in Both S_0 and S_1 Electronic States^a

	S_0	S_1
A (cm^{-1})	0.0352912(27)	0.0349400(27)
B (cm^{-1})	0.0101269(7)	0.0100983(7)
C (cm^{-1})	0.0091991(5)	0.0091132(6)
band center (cm^{-1})		35996.99(5)
A, %		69
B, %		18
C, %		13
number of assignments		274
standard deviation (MHz)		10

^{a} The wavenumber of the band center, the percentage of band type, the number of assigned lines, and the global standard deviation of the fit are also reported. The number in parentheses represents the error expressed in units of the last digit. The standard deviation for the frequency of the assigned transitions is averaged over all the 274 assignments made.

present in the R branch ended up with a safe assignment of more than 250 single eigenstate transitions in the rovibronic spectrum. We have decided to restrict the assignment to the experimental spectral lines with intensity larger than 1% of the strongest transition and to single simulated lines that are stronger than 1% of the most intense one (actually the weakest transition assigned is about 10% intensity of the strongest one). The overall quality of the best fit spectrum has been checked by computing its cross-correlation with the experimental spectrum; the obtained value is of the order of 95% of the experimental spectrum autocorrelation value.

The structural parameters obtained from the assignment of the spectrum are collected in Table 1.

COMPUTATIONAL RESULTS

As a first step, an extensive sampling of the intermolecular PES of the anisole dimer has been performed with a molecular dynamics simulation in the NVT (constant number of particles, volume, and temperature) thermodynamical ensemble, and all possible minima have been located by quenching about 5000 regularly sampled structures.[52−57] The temperature was set to 300 K, and the simulation box had a 25 Å side cube. Such a temperature is sufficient to guarantee the breaking and re-forming of the complex several times during the simulation, and the box is large enough to allow for the complete separation of the two units. The evolution of the system was calculated at a 1 fs time resolution, and the configuration sampling was occurring with a 5 ps period. The atomic point charges (available upon request) have been obtained by a fit of the electrostatic potential obtained with B3LYP/6-31G(d,p) calculations. The conjugate gradient method has been used for the minimization. At the end of the procedure we were able to obtain 18 different geometries, and we have then chosen among them the seven structures having a probability larger than 7%. Such preliminary geometries of the complex have been further reoptimized at the DFT level (M05-2X/N07D(C-Diff)) and converge to two different H-bonded structures (see Figure 3), with phenol acting as a proton donor and anisole as a proton acceptor, via its methoxy group (structure I), or π electronic density on the aromatic ring (structure II). Additionally, the possibility of stacking interactions has been considered (structure III), and in such a way three
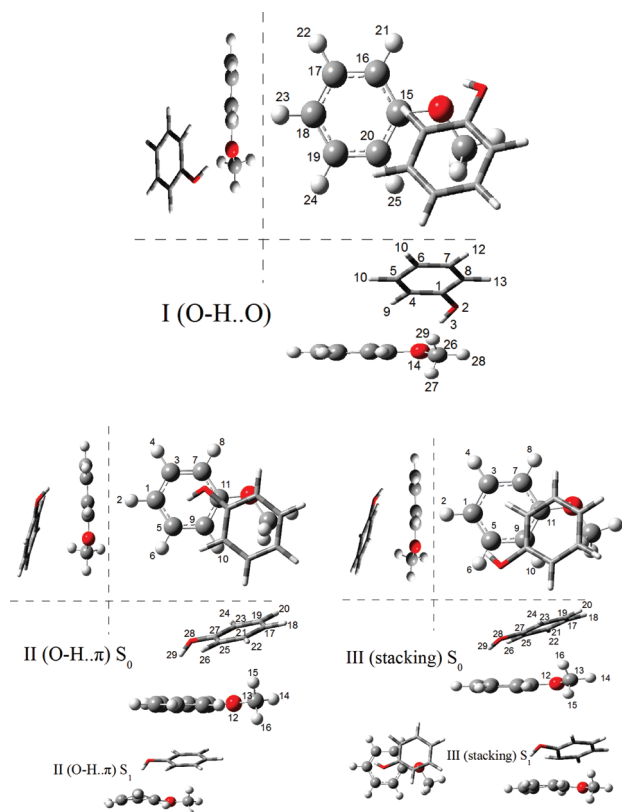
origin band around 36000 cm^{-1} is shown and the complete lack of signals at lower energy excitation is evident.

In Figure 2 the HR-LIF spectrum of the origin band of the $S_1 \leftarrow S_0$ electronic transition is reported. It has been analyzed using the JB95 program.[51] It is worth mentioning that, under our usual experimental conditions, the rotational temperature of the molecules in the beam is of the order of 4 K. In the current case (small values of rotational constants) this leads to a very congested spectrum in which almost every line is related to more than one rovibronic transition. Moreover, as already reported for the anisole dimer,[28] experimental spectra show a very complex pattern with data affected by larger errors on the intensity scale than on the frequency scale. Thus we prefer to use, whenever possible, a manual line by line assignment rather than an automated procedure based, e.g., on genetic algorithms. As a consequence, a direct experimental determination of the orientation of the transition dipole in the complex is precluded and we resorted to the orientation issuing from QM computations for the energy minimum giving the best agreement with the experimental rotational constants. Next, an iterative strategy of subsequent fittings and simulations starting from the strongest lines

9606

dx.doi.org/10.1021/jp200444a |J. Phys. Chem. A 2011, 115, 9603–9611

Figure 3. Atom numbering and geometries of the three local minima of the anisole–phenol complex in the ground state, optimized at the M05-2X/N07D(C-Diff) level. For structures II and III, geometries in the first excited electronic state, optimized at the TD-M05-2X/N07D(C-Diff) level, are also presented.

Table 2. Comparison between the Experimental Rotational Constants for the Electronic Ground State and Their Counterparts Issuing from M05-2X/N07D(C-diff) Computations for the Three Different Equilibrium Structures

S_0	experimental	I (O−H···O)	II (O−H···π)	III (stacking)
A (cm^{-1})	0.0352912(27)	0.0367542	0.0339721	0.0321614
B (cm^{-1})	0.0101269(7)	0.0102426	0.0142783	0.0147848
C (cm^{-1})	0.0091991(5)	0.0094080	0.0129196	0.0125471
MAE (%)		2.5	28.4	30.4

Table 3. Comparison between the Experimental Rotational Constants for the First Singlet Electronic Excited State and Their Counterparts Issuing from TD-M05-2X/N07D(C-diff) Computations for the Three Different Equilibrium Structures

S_1	experimental	I (O−H···O)	II (O−H···π)	III (stacking)
A (cm^{-1})	0.0349400(27)	0.0347829	0.0349740	0.0314809
B (cm^{-1})	0.0100983(7)	0.0105963	0.0146453	0.0206862
C (cm^{-1})	0.0091132(6)	0.0095210	0.0131481	0.0177403
MAE (%)		3.2	29.7	69.7

Table 4. Selected Intermolecular Parameters (distances in Å and angles in degrees) for the Three Different Equilibrium Structures in Both the Ground and First Excited Electronic States Computed at the M05-2X/N07D(C-diff) and TD-M05-2X/N07D(C-diff) Levels, Respectively

	parameter	S_0	S_1	$\Delta(S_1 - S_0)$
I (O−H···O)	O2−H3	0.969	0.980	0.011
	O14−H3	1.904	1.785	−0.119
	O2−O14	2.822	2.741	−0.081
	O2−C1	1.359	1.328	−0.031
	O2−H3−O14	157.2	164.3	7.2
	C1−O2−O14	106.0	113.0	7.0
	O2−O14−C15	125.8	121.2	−4.7
	C1−O2−O14−C26	−70.5	−79.4	−8.9
II (O−H···π)	O28−H29	0.965	0.980	0.015
	O28−C5	3.501	3.024	−0.477
	H29−C5	2.637	2.119	−0.518
	C13−C21	4.083	3.864	−0.219
	O12−C27	3.753	4.171	0.418
	C1−C5−C9	121.05	109.18	−11.9
	C11−O12−O28−C27	−42.14	−34.08	8.1
	C1−C5−C9−C11	0.43	37.98	37.5
III (stacking)	O28−O12	4.706	4.175	−0.532
	O12−C27	4.122	3.268	−0.854
	O28−C11	4.047	3.269	−0.778
	C1−C27	3.618	4.653	1.034
	C9−C5−O28	76.8	81.5	4.7
	H29−O28−H26	57.3	64.1	6.8
	C1−C11−O12−O28	108.7	136.4	27.7

different local minima have been identified for the anisole–phenol complex in its ground electronic state, and subsequently considered as starting points for geometry optimizations in the excited electronic states. It should be noted that even if an extensive PES sampling has been performed, the main goal of our study is to determine the experimentally observed structure, and not to establish all possible local minima for the anisole–phenol complex. Figure 3 shows structures I−III for the complex in its ground electronic state, as well as the excited state geometries for structures II and III. The computed rotational constants in the ground and first excited electronic state, for three different equilibrium structures, are listed in Tables 2 and 3, respectively. The mean absolute errors (MAE), the percentage of the difference between computed and experimental values of rotational constants, with respect to the experimental one, are also reported. The corresponding most relevant intermolecular parameters in the ground and first excited electronic state, along with their changes upon electronic excitation are listed in Table 4. More details on the three equilibrium structures can be obtained from their Cartesian coordinates provided in the Supporting Information. Moreover, for all geometries, the electronic excitations have been described via changes in atomic charges obtained from the NBO analysis, showing the localized character (on the phenol (94%) and anisole (93%) frames, respectively) for the structures I and II and delocalized (about 50% on each frame) character for structure III. Such results can be visualized by the plots of electron density differences between the first excited and

the ground electronic states as shown in Figure 4. For the experimentally observed structure I (vide infra) electronic excitation localized on phenol moiety leads to the strengthening of hydrogen bond, in line with elongation of the O2−H3 bond,
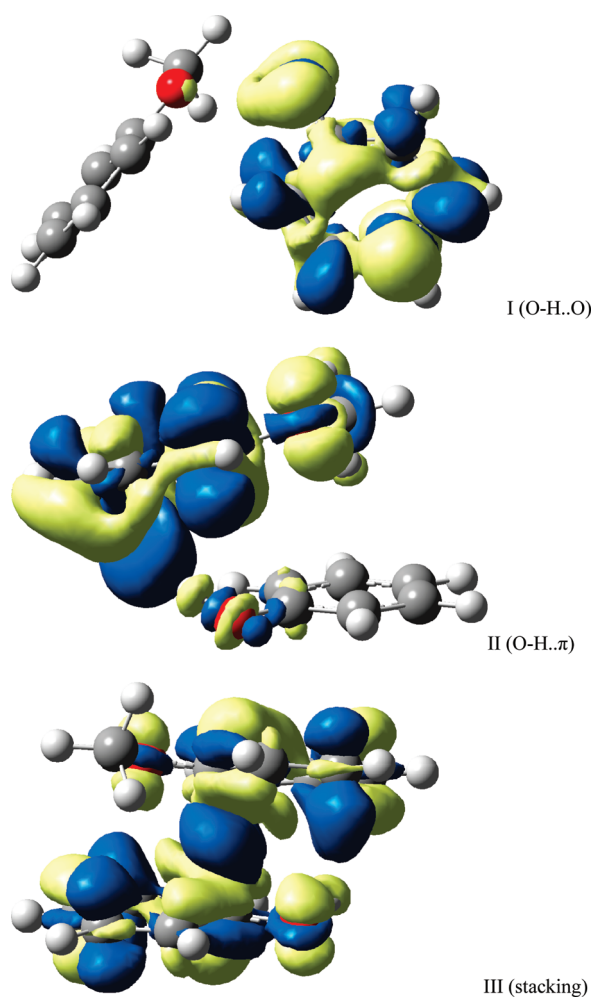
I (O-H..O)

II (O-H..π)

III (stacking)

Figure 4. Plots of the electron density differences (ELD) between the S_1 and S_0 electronic states for three different equilibrium structures, obtained with TD-M05-2X/N07D(C-diff) calculations for the structures optimized in the first excited electronic states. The regions, which have lost electron density as a result of transition, are shown in bright yellow, whereas the darker blue regions gained electron density. ELD densities evaluated with an isovalue threshold of 0.0004.

Table 5. Relative Stability of the Three Different Equilibrium Structures in Both the Ground and First Excited Electronic States Computed at the M05-2X and the TD-M05-2X Levels with the N07D(C-Diff) and N07T Basis Sets

M05-2X		S_0		
		I (O—H···O)	II (O—H···π)	III (stacking)
N07D(C-Diff)	E_{rel}(kJ/mol)	0.0	6.1	3.6
	+ZPVE	0.0	4.0	2.0
	+BSSE	0.0	4.4	2.4
N07T	E_{rel}(kJ/mol)	0.0	5.9	3.8
	+ZPVE[a]	0.0	3.8	2.3
	+BSSE	0.0	4.0	2.4

TD-M05-2X		S_1		
		I (O—H···O)	II (O—H···π)	III (stacking)
N07D(C-Diff)	E_{rel}(kJ/mol)	0.0	−2.9	−47.1
	+ZPVE	0.0	−1.3	−38.5
N07T	E_{rel}(kJ/mol)	0.0	−0.9	−44.2
	+ZPVE[a]	0.0	0.8	−35.5
	+BSSE	0.0	−0.5	−34.5/−34.4[b]

[a] Zero point vibrational energy (ZPVE) corrections from the computations with N07D(C-Diff) basis set. [b] BSEE correction obtained assuming excited anisole or phenol moiety, both values are shown (anisole*/phenol*).

the aromatic ring of anisole in the complex is no longer planar as shown by the increase of the C1—C5—C9—C11 dihedral angle from near 0 to about 38°. For structure III, no specific H-bond-like interactions can be observed, and by analogy with the benzene and anisole dimers, its geometry can be described as "displaced stacking". In this case a delocalized electronic excitation leads to geometry changes which favor larger overlap between electronic densities of both moieties. Significant differences in the structure of the complex are pointed out by the significant deviations of parameters listed in Table 4 and may be qualitatively described as a shorter intermolecular distance coupled to changes in relative orientation of both aromatic rings.

Let us now analyze the results related to the energetic properties and intermolecular interactions in anisole—phenol dimer. Relative energies reported in Table 5 show that in the ground electronic state structure I is more stable than structures II and III by about 2.5 and 4 kJ/mol, respectively. In the first excited electronic state structures I and II become essentially isoenergetic and significantly less stable than structure III. Further analysis of the intermolecular interactions in anisole—phenol dimer (see Table 6) shows a red shift of the electronic band origin (with respect to both phenol and anisole monomers) for all structures, this effect being associated with a larger binding energy in the excited state. The most pronounced red-shift (about 4000 cm^{-1}) has been predicted for structure III, in line with an increase of the interaction energy by more than 40 kJ/mol. As a matter of fact, electron excitation leads to more diffuse π-electron densities and this, in turn, allows a more stable stacking interaction between the two aromatic frames. It should be noted that the good qualitative agreement between observed and computed red shift for structure I (a few hundreds of wavenumbers in both cases) implies a correct reproduction of

shortening of the H3—O14 and O2—O14 distances, and increase of the O2—H3—O14 angle. Additionally, changes in the geometry structure suggest a weakening of the secondary interaction between π-electron density of phenol and hydrogen atoms from the anisole methyl group. Such an effect is best described by a variation of the relative position of aromatic rings from slightly tilted to almost perpendicular (e.g., the C1—O2—O14—C26 dihedral angle increases from 70.5 to 79.5°). Structure II is stabilized by the interaction between phenol acting as a proton donor and acceptor π-electronic density of the anisole, in conjunction with the interaction between the O—CH$_3$ group of anisole and phenol π-electronic density. In this case the electronic excitation leads to pronounced differences in the structure of the complex, geometry changes can be represented by a decrease of O28—C5 and H29—C5 distances by about 0.5 Å, and analogous increase of the O12—C27 distance; in line with the excitation localized on anisole characterized by a decrease of electron density on its oxygen atom and increase on the aromatic ring. Additionally,

9608

dx.doi.org/10.1021/jp200444a |*J. Phys. Chem. A* 2011, 115, 9603–9611

Table 6. Interaction Energies (in kJ/mol), $S_1 \leftarrow S_0$ Transitions (in cm^{-1}), and Their Relative Shift with Respect to Anisole or Phenol Monomers (in cm^{-1}), for the Three Different Equilibrium Structures in Both the Ground and the First Excited Electronic States Computed at the M05-2X/N07T and the TD-M05-2X/N07T Levels, Respectively[a]

	I (O−H···O)	II (O−H···π)	III (stacking)
		S_0	
ΔE (kJ/mol)	−28.5	−22.6	−24.7
+ZPVE	−22.7	−18.8	−20.4
+BSSE	−21.7	−17.7	−19.3
		S_1	
ΔE(kJ/mol)	−36.2	−36.8	−80.1/−80.5
+ZPVE	−31.9	−29.1	−65.5/−67.5
+BSSE	−30.6	−27.8	−63.1/−65.1
		$S_1 \leftarrow S_0$	
E (cm^{-1})	41400	40828	37383
+ZPVE	41383	40815	37376
+BSSE	41489	40928	37571/37576
ΔE (cm^{-1})	−643	−1186	−4631/−4661
+ZPVE	−772	−860	−3766/−3933
+BSSE	−748	−846	−3661/−3827

[a] Zero point vibrational energy (ZPVE) corrections from computations with N07D(C-Diff) basis set. For the stacking structure with delocalized electronic excitation the relative shifts and interaction energies have been computed assuming both possibilities for monomer excitation. Thus energies with respect to anisole monomer in excited state and phenol in the ground state (A*+Ph) and anisole in the ground state with phenol in its excited state (A+Ph*) have been computed and both values are shown (A*+Ph/A+Ph*).

the changes in the interaction energy issuing from electronic excitation but does not have any direct relationship with the absolute value of the binding energy, which is, in fact, quite difficult to estimate. Thus, taking into account the comparison of the M05-2X/TD-M05-2X results with the ground state SAPT (symmetry-adapted intermolecular perturbation theory) computations or evaluation of ground and/or excited state interaction energies at coupled cluster level for other weakly bounded complexes of anisole,[28,58] we assume that the interaction energies reported in Table 6 could be slightly overestimated and should be considered as the upper limits.

■ DISCUSSION

Comparison of the experimentally obtained rotational constants with the calculated ones (see Tables 2 and 3) strongly suggests that the equilibrium structure of the anisole−phenol complex should be the one that is stabilized by a hydrogen bond involving phenol as the proton donor and the oxygen of the anisole methoxy group as the proton acceptor. As already reported for the phenol dimer[23,24] and discussed above, also in this case it is possible to recognize a stabilizing contribution due to the π−π interaction between the two aromatic rings. This is the reason why the two aromatic rings partially overlap.

As is well-known, the frequency shift of the band origin observed for the complex, with respect to the bare chromophores, combined with a sound knowledge of the nature of the
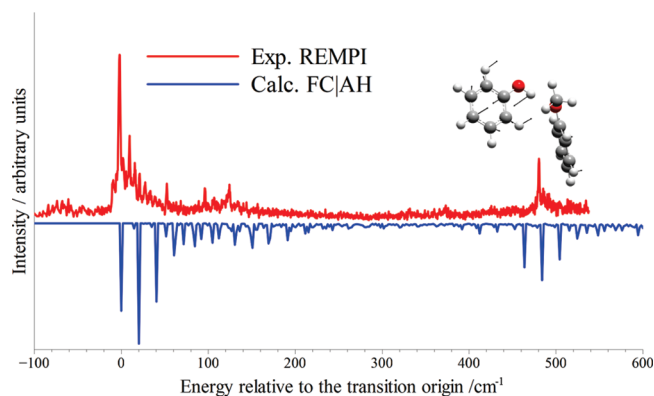

Figure 5. Comparison between computed and experimental REMPI spectrum of the anisole−phenol complex. Both spectra are reported in the energy scale relative to the 0−0 electronic transition. For the computed spectrum anharmonic effects have been taken into account by scaling the harmonic vibronic energies by 0.92.

transition, can give information about the interactions that stabilize the complex. In this respect, the TD-DFT calculations performed in this work show that, for structure I, the $S_1 \leftarrow S_0$ electronic transition is localized on the phenol molecule and has a $(n,\pi) \rightarrow \pi^*$ character: relative changes in the electron density make phenol more "acid", and the interactions involving it as proton donor become stronger, fully in line with the observed red shift. Additionally, the experimentally recorded spectrum and the one simulated within Franck−Condon Adiabatic Hessian (FC|AH) framework for structure I, which are presented in Figure 5, show very good agreement. In fact the spectrum features are correctly reproduced by simulation, both spectra showing the rich structure in the region below 200 cm^{-1} from the band origin and the strong band around 500 cm^{-1}, which can be assigned to an in-plane deformation of the phenol ring. Thus, an overall comparison between experimental and theoretical results confirms that the O−H···O structure, with the electronic excitation localized on the phenol, has been experimentally observed.

However, in analogy with the phenol dimer one would expect a second strong band related to the transition origin localized on the anisole moiety, which has not been identified in the current experiments. One possible explanation is that the intensity of the missing transition is significantly lower and thus it remains hidden in the background of the experimental spectrum. Such a possibility can be examined by computation of the Franck−Condon factors, which has been performed within the vertical approximation due to the fact that, despite extensive computations, a structure corresponding to the O−H···O interaction with the excited state localized on the anisole frame has not been found. The (FC|VG) computations confirmed that the FC factors related to the transition localized on anisole ($S_2 \leftarrow S_0$) are 3 orders of magnitude lower than the ones obtained for the observed $S_1 \leftarrow S_0$ band. Such low FC factors are mainly due to the dominant component of the shift vector **K**, connected with the lowest intermolecular vibration, which can be described as O−H···O ↔ O−H···π isomerization coordinate. To validate the above-mentioned analysis, analogous computations have been performed for the phenol dimer. In this case, FC|VG computations lead to large FC factors for both transitions, localized on the donor and acceptor phenol moieties, fully in line with the observation of two separate electronic transition origins.
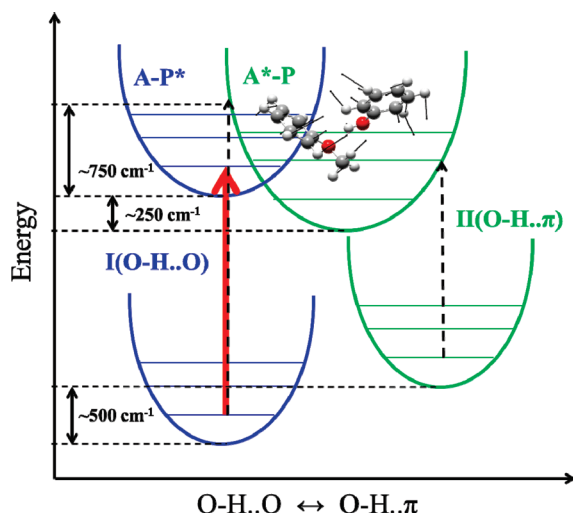
Figure 6. Schematic representation of the ground and excited states PES of the anisole−phenol complex. Structures I and II and the electronic transitions localized on the phenol or anisole frames (marked by asterisk) are considered. Arrows represent possible electronic transitions, the experimentally observed transition is shown as a red solid arrow, and the transitions which have not been observed in the current experiment by black dashed arrows. Intermolecular vibration with the largest component of the shift vector **K**, as obtained through FC|VG computations for $S_2 \leftarrow S_0$ transition, is also presented. Some relative energies indicated in the scheme are obtained from computations at the (TD-)M05-2X//N07D(C-diff) level.

It is also worth discussing the possibility of another electronic transition related to structures II and III, which should be also taken into account in view of the comparable stabilization energies. In this case computational results suggest that for both of them the electronic transition origins should be shifted to lower energies (with respect to monomers) by about 1000 and 4000 cm^{-1}, respectively. On these grounds, we have further checked a region red-shifted by up to 1200 cm^{-1} with respect to the band origin assigned to the $S_1 \leftarrow S_0$ excitation localized on the phenol frame. One possible reason for the lack of a second band origin could be related to a kinetic rather than thermodynamic control in the formation of the phenol−anisole complex so that not all the possible complex structure would be actually present in the molecular beam. Another explanation is, instead, related to the very small Franck−Condon factors computed at the FC|AH level for the vibrational ground states of structures II and III. Such findings are in line with large geometry changes upon electronic transition and suggest that, even if potentially present in the molecular beam, both stacking and O−H···π structures would not be observed in the current experiment.

Experimental studies supported by extensive computations lead to a clear and self-consistent picture of the ground and excited states potential energy hypersurfaces of the anisole−phenol complex, which can be qualitatively illustrated by the scheme reported in Figure 6. It is suggested that, upon electronic excitation of the global minimum hydrogen bonded structure, it is possible to reach the A*−P PES far from equilibrium, leading to the complex bound through O−H···π interaction. Thus, the excitation localized on the anisole may in turn lead to changes in the structure of the complex, allowing a photoinduced isomerization process, and explaining the absence of the second band origin in the observed spectrum.

CONCLUSIONS

The origin of the $S_1 \leftarrow S_0$ electronic transition for the anisole−phenol complex has been localized using REMPI spectroscopy studies. The structure of the complex observed in the REMPI experiment has been elucidated by comparison of HR-LIF and computational data. The remarkable agreement between computed and experimental rotational constants allowed the structure of the complex to be resolved and to identify the main stabilizing interactions occurring between the two partners, i.e., a hydrogen bond with the phenol acting as proton donor toward the anisole oxygen atom. Additionally, the computation of electronic properties in the excited state has provided information about the character of the transition, localized on the phenol moiety, while the good agreement between experimental and simulated spectra further confirmed that the band observed at 35996.99 cm^{-1} should be related to a hydrogen-bonded structure of the complex. Moreover, extensive computational studies allowed further insights to be gained about the possible photoinduced processes in the anisole−phenol complex and provided a convincing explanation for the observation of just a single electronic transition in the current experiment.

ASSOCIATED CONTENT

S **Supporting Information.** Cartesian coordinates for structure I, II, and III of the anisole−phenol cluster in the ground and the first electronically excited state computed at the (TD-)M05-2X/N07D(C-Diff) level. This material is available free of charge via the Internet at http://pubs.acs.org.

AUTHOR INFORMATION

Corresponding Author
*E-mail: gianni.pietraperzia@unifi.it, malgorzata.biczysko@sns.it.

Present Addresses
⊥Now at LFP—Laboratoire Francis Perrin, CEA-CNRS, CEA Saclay, France.

ACKNOWLEDGMENT

REFERENCES

(1) Mulliken, R. S. *J. Am. Chem. Soc.* **1952**, 74, 811.
(2) Hunter, C. A.; Sanders, J. K. M. *J. Am. Chem. Soc.* **1990**, 112, 5525.
(3) Kumph, R. A.; Dougherty, D. A. *Science* **1993**, 261, 1708.
(4) Meyer, E. A.; Castellano, R. K.; Diederich, F. *Angew. Chem., Int. Ed.* **2003**, 42, 1210.
(5) Johnson, E. R.; Keinan, S.; Mori-Sanchez, P.; Contreras-Garcia, J.; Cohen, A. J.; Yang, W. *J. Am. Chem. Soc.* **2010**, 132, 6498.
(6) Zhu, H.; Sommer, I.; Lengauer, T.; Domingues, F. S. *PLoS* **2008**, 3, e1926.
(7) Knowles, R. R.; Jacobsen, E. N. *Proc. Natl. Acad. Sci. U.S.A.* **2010**, 107, 20678.
(8) Saccomandi, G.; Sgura, I. *J. R. Soc. Interface* **2006**, 3, 655.

(9) Cooper, V. R.; Thonhauser, T.; Pudzer, A.; Schröder, E.; Lundqvist, B. I.; Langreth, D. C. *J. Am. Chem. Soc.* **2008**, *130*, 1304.

(10) Marsili, S.; Chelli, R.; Schettino, V.; Procacci, P. *Phys. Chem. Chem. Phys.* **2008**, *10*, 2673.

(11) Grimme, S. *Angew. Chem., Int. Ed.* **2008**, *47*, 3430.

(12) Williams, D. H.; Stephens, E.; O'Brien, D. P.; Zhou, M. *Angew. Chem., Int. Ed.* **2004**, *43*, 6596.

(13) Nooren, I. M. A.; Thornton, J. M. *EMBO J.* **2003**, *22*, 3486.

(14) Arunan, E.; Gutawsky, H. S. *J. Chem. Phys.* **1993**, *98*, 4294.

(15) Thonhauser, T.; Pudzer, A.; Langreth, D. C. *J. Chem. Phys.* **2006**, *124*, 164106.

(16) Chipot, C.; Ja_e, R.; Maigret, B.; Pearlman, D. A.; Kollman, P. A. *J. Am. Chem. Soc.* **1996**, *118*, 11217.

(17) Gervasio, F. L.; Chelli, R.; Procacci, P.; Schettino, V. *J. Phys Chem. A* **2002**, *106*, 2945.

(18) Ishikawa, S.; Ebata, T.; Inoue, T.; Mikami, N. *J. Phys. Chem.* **1996**, *100*, 10531.

(19) Dopfer, O.; Lembach, G.; Wright, T. G.; Müller-Dethlefs, K. *J. Chem. Phys.* **1993**, *98*, 1933.

(20) Fang, W. H. *J. Chem. Phys.* **2000**, *112*, 1204.

(21) Weichert, A.; Riehn, C.; Brutschy, B. *J. Phys. Chem. A* **2001**, *105*, 5679.

(22) Ebata, T.; Wanatabe, T.; Mikami, N. *J. Phys. Chem.* **1995**, *99*, 5761.

(23) Schmitt, M.; Bohm, M.; Ratzer, C.; Krugel, D.; Kleinermanns, K.; Kalman, I.; Berden, G.; Meerts, W. L. *Chem. Phys. Chem.* **2006**, *7*, 1241.

(24) Brause, R.; Santa, M.; Schmitt, M.; Kleinermanns, K. *Chem. Phys. Chem.* **2007**, *8*, 1394.

(25) Pasquini, M.; Schiccheri, N.; Piani, G.; Pietraperzia, G.; Becucci, M.; Biczysko, M.; Pavone, M.; Barone, V. *J. Phys. Chem. A* **2007**, *111*, 12363.

(26) Piani, G.; Pasquini, M.; Pietraperzia, G.; Becucci, M.; Armentano, A.; Castellucci, E. *Chem. Phys. Lett.* **2007**, *434*, 25.

(27) Biczysko, M.; Piani, G.; Pasquini, M.; Schiccheri, N.; Pietraperzia, G.; Becucci, M.; Pavone, M.; Barone, V. *J. Chem. Phys.* **2007**, *127*, 144303.

(28) Pietraperzia, G.; Pasquini, M.; Schiccheri, N.; Piani, G.; Becucci, M.; Castellucci, E.; Biczysko, M.; Bloino, J.; Barone, V. *J. Phys. Chem. A* **2009**, *113*, 14343.

(29) Schiccheri, N.; Pasquini, M.; Piani, G.; Pietraperzia, G.; Becucci, M.; Biczysko, M.; Bloino, J.; Barone, V. *Phys. Chem. Chem. Phys.* **2010**, *12*, 13547.

(30) Kerstel, E. R. Th.; Becucci, M.; Pietraperzia, G.; Castellucci, E. *Chem. Phys.* **1995**, *199*, 263.

(31) Becucci, M.; Pietraperzia, G.; Pasquini, M.; Piani, G.; Zoppi, A.; Chelli, R.; Castellucci, E.; Demtroeder, W. *J. Chem. Phys.* **2004**, *120*, 5601.

(32) Pasquini, M.; Piani, G.; Pietraperzia, G.; Demtroeder, W.; Giuntini, M.; Becucci, M. *Rev. Sci. Instrum.* **2005**, *76*, 113105.

(33) Zhao, Y.; Schults, N. E.; Truhlar, D. G. *J. Chem. Theory Comput.* **2006**, *2*, 364.

(34) Jacquemin, D; Perpète, E. A.; Ciofini, I.; Adamo, C.; Valero, R.; Zhao, Y.; Truhlar, D. G. *J. Chem. Theory Comput.* **2010**, *6*, 2071.

(35) Jacquemin, D; Perpète, E. A.; Ciofini, I.; Adamo, C. *J. Chem. Theory Comput.* **2010**, *6*, 1532.

(36) Zhao, Y.; Truhlar, D. G. *Chem. Phys. Lett.* **2011**, *502*, 1.

(37) Zhao, Y.; Truhlar, D. G. *Theor. Chim. Acta* **2008**, *120*, 215.

(38) Barone, V.; Cimino, P.; Stendardo, E. *J. Chem. Theory Comput.* **2008**, *4*, 751.

(39) Barone, V.; Cimino, P. *Chem. Phys. Lett.* **2008**, *454*, 139.

(40) Double and triple-ζ basis sets of N07 family; IDEA: In-Silico Developments for Emerging Applications; http://idea.sns.it. Accessed January 7, 2011.

(41) Barone, V.; Bloino, J.; Biczysko, M. *Phys. Chem. Chem. Phys.* **2010**, *12*, 1092.

(42) Scalmani, G.; Frish, M. J.; Menucci, B.; Tomasi, J.; Cammi, R.; Barone, V. *J. Chem. Phys.* **2006**, *124*, 094107.

(43) Barone, V.; Bloino, J.; Biczysko, M.; Santoro, F. *J. Chem. Theory Comput.* **2009**, *5*, 540.

(44) Bloino, J.; Biczysko, M.; Santoro, F.; Barone, V. *J. Chem. Theory Comput.* **2010**, *6*, 1256.

(45) Duschinsky, F. *Acta Physicochim. URSS* **1937**, *7*, 551.

(46) Santoro, F.; Improta, R.; Lami, A.; Bloino, J.; Barone, V. *J. Chem. Phys.* **2007**, *126*, 084509.

(47) Santoro, F.; Lami, A.; Improta, R.; Bloino, J.; Barone, V. *J. Chem. Phys.* **2008**, *128*, 224311.

(48) Macak, P.; Luo, Y.; Ågren, H. *Chem. Phys. Lett.* **2000**, *330*, 447.

(49) Reed, A. E.; Curtiss, L. A.; Weinhold, F. *Chem. Rev.* **1988**, *88*, 899.

(50) Frisch, M. J.; Trucks, G. W.; Schlegel, H. B.; Scuseria, G. E.; Robb, M. A.; Cheeseman, J. R.; Scalmani, G.; Barone, V.; Mennucci, B.; Petersson, G.; Nakatsuji, H.; Caricato, M.; Li, X.; Hratchian, H. P.; Izmaylov, A. F.; Bloino, J.; Zheng, G.; Sonnenberg, J. L.; Hada, M.; Ehara, M.; Toyota, K.; Fukuda, R.; Hasegawa, J.; Ishida, M.; Nakajima, T.; Honda, Y.; Kitao, O.; Nakai, H.; Vreven, T.; Montgomery, J. A.; Peralta, J. E.; Ogliaro, F.; Bearpark, M.; Heyd, J. J.; Brothers, E.; Kudin, K. N.; Staroverov, V. N.; Kobayashi, R.; Normand, J.; Raghavachari, K.; Rendell, A.; Burant, J.; Iyengar, S. S.; Tomasi, J.; Cossi, M.; Rega, N.; Millam, J. M.; Klene, M.; Knox, J. E.; Cross, J. B.; Bakken, V.; Adamo, C.; Jaramillo, J.; Gomperts, R.; Stratmann, R. E.; Yazyev, O.; Austin, A. J.; Cammi, R.; Pomelli, C.; Ochterski, J. W.; Martin, R. L.; Morokuma, K.; Zakrzewski, V. G.; Voth, G. A.; Salvador, P.; Dannenberg, J.J.; Dapprich, S.; Parandekar, P. V.; Mayhall, N. J.; Daniels, A. D.; Farkas, O.; Foresman, J. B.; Ortiz, J. V.; Cioslowski, J.; Fo, D. J. *Gaussian 09, Revision A.02*; Gaussian, Inc.: Wallingford, CT, 2009.

(51) Plusquellic, D. F., http://physics.nist.gov/jb95, NIST: Gaithersburg, MD, 2003.

(52) Kratochvil, M.; Sponer, J.; Hobza, P. *J. Am. Chem. Soc.* **2000**, *122*, 3495.

(53) Ryjaek, F.; Kratochvil, M.; Hobza, P. *Chem. Phys. Lett.* **1999**, *313*, 393.

(54) Kratochvil, M.; Engkvist, O.; Jungwirth, P.; Hobza, P. *Phys. Chem. Chem. Phys.* **2000**, *2*, 2419.

(55) Kratochvil, M.; Engkvist, O.; Sponer, J.; Jungwirth, P.; Hobza, P. *J. Phys. Chem. A* **1998**, *102*, 6921.

(56) Ryjaek, F.; Engkvist, O.; Vacek, J.; Kratochvil, M.; Hobza, P. *J. Phys. Chem. A* **2001**, *105*, 1197.

(57) Gervasio, F. L.; Procacci, P.; Cardini, G.; Guarna, A.; Giolitti, A.; Schettino, V. *J. Phys. Chem. B* **2000**, *104*, 1108.

(58) Barone, V.; Biczysko, M.; Pavone, M. *Chem. Phys.* **2008**, *346*, 247.

9611

dx.doi.org/10.1021/jp200444a |*J. Phys. Chem. A* 2011, 115, 9603–9611